Rijksuniversiteit Groningen

Bachelor Thesis

Department of Mathematics and Natural Sciences

Observing Lorentz Invariance Violation In Weak Interaction

Author:
Adam Watson

Supervisors:
Prof. Hans Wilschut
Prof. Rob Timmermans

July 8, 2016

Contents

Chapter 1

Introduction

1.1 Motivation

The study of Lorentz invariance violation (LIV) is motivated by certain predictions made by theories of quantum gravity (see for example [9]). These include the possibility of spontaneous breaking of Lorentz invariance. Such effects go beyond relativistic theories, which require invariance under Lorentz transformations (boosts and rotations). In addition to Lorentz symmetry, there is also the related concept of CPT symmetry. The latter is violated if Lorentz-invariance is violated, but the converse does not necessarily hold. These symmetries are conserved in the Standard Model (SM) of particle physics, and in general relativity (GR). Unification of these theories is a major goal of theoretical high energy physics. The energies at which unification will occur is expected to be at the Planck scale, 17 orders of magnitude larger than the electroweak scale. Such large energies preclude direct experiments to test these unification theories. However, if there are new, as yet unknown, interactions at an energy scale beyond that of the electroweak scale, there may be "windows" on quantum gravity, which may have phenomenological consequences at lower energies (such as LIV). In this thesis, we study the possibility of experimentally observing rotational-LIV, by looking at the distribution of gamma radiation of polarized nuclei following β-decay.

The underlying physics of quantum gravity are unknown. For this reason, it is useful to use an effective field theory (EFT) approach that includes all possible Lorentz-violating operators. One such EFT is the Standard Model Extension (SME) (see for example [3]). In this study we focus on a restricted

number of Lorentz-violating coefficients, which are parametrized by a general tensor $\chi_{\mu\nu}$. This tensor is added to the W-boson propagator, which then assumes the form (at low energies) [11]

$$< W^{\mu+}(p)W^{\nu-}(-p) >= \frac{i(g^{\mu\nu} + \chi^{\mu\nu})}{M_W^2} \tag{1.1}$$

where $g^{\mu\nu}$ is the Minkowski metric and $\chi^{\mu\nu}$ is the general Lorentz-violating tensor. We aim to improve the current upper bounds on certain components of $\chi^{\mu\nu}$. The reason we look at β-decay is because it is a well recognised probe of symmetry violation in the weak interaction.

1.2 Outline

In Chapter 2 the outline of β-decay is presented, followed by a description of the correlation coefficients that link different observables in β-decay, such as β momentum and nuclear spin. In this study we assume the validity of the Standard Model, and therefore all coefficients that are zero in this framework are excluded. The correlation coefficients that are left will then depend upon SM couplings. We then take Treiman's [12] claim, that nuclei undergoing β-decay can become polarized along their recoil axis, and derive the m-state distribution of the daughter nucleus relative to the recoiling nucleus. Here we do not assume any LIV.

In Chapter 3, the theory of nuclear orientation following β-decay is developed. This is useful in order to establish the asymmetries that can be measured to test for LIV. The γ-ray distribution of the daughter nucleus along the recoil direction is derived and plotted for two radioactive isotopes; cobalt-60 and sodium-22. A weak deviation from isotropy is found in both isotopes. In addition, we analyse the effect on nuclear orientation and γ-ray distribution by assuming a tensor ($\mathbf{T}$) component in the weak interaction.

In Chapter 4, we derive the decay rate distribution of γ-radiation of polarized nuclei using the LIV formalism. By analogy with the Treiman claim, the recoil direction along which the γ-distribution is measured is defined along the preferred direction in space. An approach similar to that of Chapter 3 is then used in order to derive the angular distribution of γ-radiation, with the inclusion of the Lorentz violating tensor. The maximal asymmetry is then calculated, and found to have a sensitivity of about 10 percent. Following

a brief statistical analysis, the detector opening angle will be optimized assuming a certain geometrical setup, as well as a discussion of the orientation of the detectors. Finally, the asymmetry oscillation as a function of sidereal time will be derived and plotted.

Chapter 2

Fundamentals of Beta-Decay

In β-decay, it is possible to measure the correlations between different observables, such as the momentum of the β particle, or the nuclear spin. The strength of the correlations can be written down in terms of what is often called the 'alphabet soup'. The various coefficients depend upon Standard Model couplings ($\mathbf{V} - \mathbf{A}$), as well as possible new V, A, S, P and T interactions. In this chapter an outline of the relevant theory of beta decay is given, followed by a description of the decay-rate distribution of polarized nuclei. A derivation of the various coefficients associated with Fermi and Gamow-Teller decays is also presented.

2.1 Beta Decay

Beta Decay is a type of radioactive decay wherein a proton is converted to a neutron, or vice versa, inside a nucleus. In the process a beta particle (either an electron or a positron) is emitted, as well as a neutrino or antineutrino. This process can be represented by a Feynman diagram (see Figure 2.1)

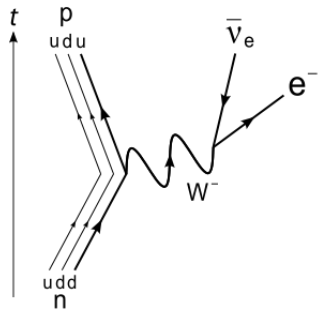

Figure 2.1: The Feynman diagram for β^- decay of a neutron into a proton, electron, and electron antineutrino.

The generic equation for β^- decay can be written as ${}^A_Z X \rightarrow {}^A_{Z+1} X' + e^- + \bar{\nu_e}$, and similarly for β^+ decay, as β^- decay can be written as ${}^A_Z X \rightarrow {}^A_{Z-1} X' + e^+ + \nu_e$.

2.1.1 Fermi Theory

It was Fermi who in 1934 proposed the first successful theory of nuclear beta decay, by analogy with the electromagnetic interaction [10]. The latter is described by a Lorentz invariant scalar transition amplitude, written as

$$\mathscr{M}_{fi} = \int \Psi_f^* (g\hat{O}) \Psi_i dV \tag{2.1}$$

Where g is a dimensionless coupling constant relevant to the interaction being considered, and Ψ_i and Ψ_f are respectively the initial and final wavefunctions for the states. It was later discovered that the weak interaction does not conserve parity, thus $|\mathscr{M}_{fi}|^2$ must be a mixture of scalar and pseudoscalar. The operator $\hat{O}$ can be in principle several Lorentz invariant forms, but for the weak interaction the only one that provides the correct helicity properties for leptons is a mixture of both vector ($\mathbf{V}$) and axial-vector ($\mathbf{A}$). Decays which proceed via $\mathbf{A}-\mathbf{A}$ are known as Gamow-Teller, and those that proceed via $\mathbf{V}-\mathbf{V}$ are known as Fermi.

2.1.2 Beta-particle energy spectrum

The probability of β-decay depends on a number of factors. These include the kinematic quantities such as the angular momentum of the emitted particles, as well as the Q value and the initial and final states of the nucleus in question. The transition rate can be written according to Fermi's Golden Rule

$$\omega = \frac{2\pi}{\hbar}|\mathscr{M}_{fi}|^2 n(E) \tag{2.2}$$

Where ω is the transition rate, and $n(E)$ is the density of states. The dynamics of the process are encoded in the transition amplitude $|\mathscr{M}_{fi}|^2$, which is related to the matrix element $|M_{fi}|$ as

$$\mathscr{M}_{fi} = \frac{G_F}{V} M_{fi} \tag{2.3}$$

Where G_F is the Fermi coupling constant, and V represents an arbitrary volume which eventually cancels with a factor in the phase-space term. To obtain the β-decay spectrum we need the differential decay rate, which for decays in which the electron has an energy in the range E_e to $E_e + dE_e$ is given as

$$d\omega = \frac{2\pi}{\hbar}|\mathscr{M}_{fi}|^2 n_\nu(E_0 - E_e) n_e(E_e) dE_e \tag{2.4}$$

Where n_e and n_ν are the density of states factors for the electron and neutrino. If we change the variable to p_e (electron momentum) and assuming the neutrino is massless such that $p_\nu = E_\nu/c$ we arrive at the following differential decay rate

$$\frac{d\omega}{dp_e} = {G_F}^2|\mathscr{M}_{fi}|^2 \frac{{p_e}^2 {E_\nu}^2}{2\pi^3\hbar^7 c^3} = {G_F}^2|\mathscr{M}_{fi}|^2 \frac{{p_e}^2 (E_0 - E_e)^2}{2\pi^3\hbar^7 c^3} \tag{2.5}$$

2.1.3 Allowed and Forbidden Transitions

We can assume that the emitted lepton wavefunctions are plane waves. Thus the matrix element $\mathscr{M}_{fi}$ will contain a factor $\exp(-i\mathbf{P}\cdot\mathbf{r}/\hbar)$. Two cases arise, known as allowed and forbidden transitions, depending on how we treat the lepton wavefunctions. This will be considered below.

Allowed Transitions

For typical values, $PR/\hbar$ is often much less than unity. Thus the exponential can be replace by 1 and the matrix element $\mathscr{M}_{fi}$ defined above will not depend on the lepton momenta, and the differential decay rate will depend only on kinematical variables via the density of states factors. For the emitted leptons $\mathbf{L} = \mathbf{0}$, but $\mathbf{S} = \mathbf{0}, \mathbf{1}$, or anti-parallel and parallel respectively. In the former case there is no change in nuclear spin ($\Delta J = 0$), and the change in parity is also zero. Processes with these properties are known as Fermi transitions. For the parallel case, $\Delta J = 0, 1$, with no parity change. These processes correspond to Gamow-Teller transitions.

Forbidden Transitions

The nucleus can change its spin by more than one unit, and there may also be a parity change between initial and final nuclear states. Often we cannot express the plane wave as unity, and we need to expand $\exp(-i\mathbf{P}\cdot\mathbf{r}/\hbar)$ in a power series in $\mathbf{P}\cdot\mathbf{r}/\hbar$. These transitions involve the lepton pair carrying away a total orbital angular momentum of of quantum number $L = 1, 2, ...$ etc. We cannot assume that the matrix element $\mathscr{M}_{fi}$ will be independent of the lepton momenta.

2.2 Correlation Coefficients in Beta-Decay

We can write the decay-rate distribution for polarized nuclei as [7]

$$\begin{aligned}
&\omega(\langle\vec{J}\rangle|E_e,\Omega_e,\Omega_\nu)dE_e d\Omega_e d\Omega_\nu \\
&= \frac{F(\pm Z,E_e)}{(2\pi)^5} p_e E_e (E_0-E_e)^2 dE_e d\Omega_e d\Omega_\nu \\
&\quad\times\bar{\xi}\left\{1 + a\frac{\vec{p}_e\cdot\vec{p}_\nu}{E_e E_\nu} + b\frac{m_e}{E_e} + c\left[\frac{1}{3}\frac{\vec{p}_e\cdot\vec{p}_\nu}{E_e E_\nu} - \frac{(\vec{p}_e\cdot\vec{j})(\vec{p}_\nu\cdot\vec{j})}{E_e E_\nu}\right]\left[\frac{J(J+1)-3\langle(\vec{J}\cdot\vec{j})^2\rangle}{J(2J-1)}\right]\right. \\
&\quad\left. + \frac{\langle\vec{J}\rangle}{J}\cdot\left[A\,\frac{\vec{p}_e}{E_e} + B\,\frac{\vec{p}_\nu}{E_\nu} + D\,\frac{\vec{p}_e\times\vec{p}_\nu}{E_e E_\nu}\right]\right\} . \qquad (2.6)
\end{aligned}$$

where $E_{e(\nu)}$, $\Omega_{e(\nu)}$, and $p_{e(\nu)}$ denote the total $\beta(\nu)$ energy, direction, and momentum, respectively, E_0 is the energy available to the electron and the

coefficient	F	GT		
polarized parent spin J	$J \to J$	$J \to J-1$	$J \to J$	$J \to J+1$
unpolarized parent daughter spin J	$J \to J$	$J-1 \to J$	$J \to J$	$J+1 \to J$
a	1	$-\frac{1}{3}$		
c	0	-1	$\frac{2J-1}{J+1}$	$-\frac{J(2J-1)}{(J+1)(2J+3)}$
A	0	∓ 1	$\mp\frac{1}{J+1}$	$\pm\frac{J}{J+1}$
B	0	± 1	$\pm\frac{1}{J+1}$	$\mp\frac{J}{J+1}$

Table 2.1: Values of the relevant correlation coefficients in Fermi and Gamow-Teller transitions. Upper (lower) sign refers to electron (positron)emission. The second row indicates how to select the parameters when discussing β decay from an unpolarized sample and observing the m state population of the daughter nucleus.

neutrino, $\langle \vec{J} \rangle$ is the expectation value of the spin of the initial nuclear state, and $\vec{j}$ is the unit vector in this direction; $F(\pm Z, E_e)$ is the Fermi function which modifies the phase space of the electron due to the Coulomb field of the nucleus. The Fierz interference term also affects the phase space, but is zero in the SM. $\bar{\xi} \equiv G_F^2 V_{ud}^2 / 2\xi$, where ξ gives the strength of the interaction. The remaining terms describe the β-correlation coefficients: the β-neutrino asymmetry a, the P-odd "Wu-parameter," i.e. the β-asymmetry A, the neutrino asymmetry B, and the triple-correlation coefficient D. Also $D = 0$ in the SM (at tree level and neglecting final state interactions). The c coefficient vanishes for non-oriented nuclei and for nuclei with $J = 1/2$, such as the neutron. To simplify matters, in this study we take $F = 1$. The expressions for the correlation coefficients in pure Fermi and G-T transitions, assuming the SM applies, are in Table 2.1. Our decay rate distribution for polarized nuclei then becomes

$$\omega(\langle m\rangle\vec{j}|E_e,\Omega_e,\Omega_\nu)dE_e d\Omega_e d\Omega_\nu$$
$$= \frac{1}{(2\pi)^5} p_e E_e (E_0 - E_e)^2 dE_e d\Omega_e d\Omega_\nu$$
$$\times \bar{\xi}\left\{1 + a\frac{\vec{p}_e\cdot\vec{p}_\nu}{E_e E_\nu} + c\left[\frac{1}{3}\frac{\vec{p}_e\cdot\vec{p}_\nu}{E_e E_\nu} - \frac{(\vec{p}_e\cdot\vec{j})(\vec{p}_\nu\cdot\vec{j})}{E_e E_\nu}\right]\left[\frac{J(J+1)-3\langle m^2\rangle}{J(2J-1)}\right]\right.$$
$$\left. + \frac{\langle m\rangle}{J}\vec{j}\cdot\left[A\frac{\vec{p}_e}{E_e} + B\frac{\vec{p}_\nu}{E_\nu}\right]\right\}\ , \tag{2.7}$$

where it is made explicit that we measure the distribution of m values on a certain axis, in this case the axis of polarization. One is free to choose any axis. What is relevant for the understanding of the Treiman approach [12] is the recoil direction. This means one can integrate Eq. 2.7 taking care that $\vec{p}_e$ and $\vec{p}_\nu$ are defined along that axis. It is impossible to know the recoil direction a priori, thus it has no practical meaning. In order to obtain the distribution along the recoil axis, one can integrate Eq. 2.7. The first two terms are independent of polarization, and integrating them gives the value X defined in Treiman [12]. The third term, associated with the coefficient c, is related to the alignment, and is even in parity. This is evaluated as $cX_2\frac{J(J+1)-3<m^2>}{J(2J-1)}(\frac{1}{3}-\cos^2(\theta))$ [12]. The last two terms are associated with the coefficients A and B. Integrating the term $A\frac{<m>}{J}\frac{\vec{j}\cdot\vec{p}_e}{E_e}$ in the recoil direction yields $-\frac{<m>}{J}AX_1\cos(\theta)$. The neutrino dependence (associated with B) yields a similar result. Normalizing to X, we have the result

$$W(\theta) = 1 - (A+B)\frac{\langle m\rangle}{J}x_1\cos\theta + c\,x_2\frac{J(J+1)-3\langle m^2\rangle}{J(2J-1)}\left(\frac{1}{3}-\cos^2\theta\right) \tag{2.8}$$

where $x_1 = X_1/X$ and $x_2 = X_2/X$. If we now look at the situation in reverse, we can ask what orientation the daughter nucleus should have, such that the parent nucleus is randomly oriented. In the original distribution function for initially oriented nuclei, we had terms of the form $<\vec{J}>\cdot\vec{q}/q$. Such terms can be reevaluated as the spin projection m along the recoil axis, defined by the vector $\vec{q}$. Thus we can define $\theta = 0$ along this axis and obtain the formula given in [6]

$$W(m) = \frac{1}{2J+1}\left[1 - (A+B)x_1\frac{m}{J} - \frac{2}{3}c\,x_2\frac{J(J+1)-3m^2}{J(2J-1)}\right] \tag{2.9}$$

With this distribution we can calculate the γ-ray pattern relative to the recoiling nucleus. Due to changing from the recoil distribution of the daughter nucleus following β-decay of oriented nuclei, to the m-state distribution of the recoiling nucleus following β-decay of unoriented nuclei (involving a reversal in the time direction), the coefficients A, B and c need to be modified. This is because we interchange the roles of J and J', were J is now the spin of the recoiling nucleus, and J' the spin of the initial nucleus. This involves changing the sign of $\lambda_{J'J}$. The values are given in Table 2.1.

Chapter 3

Orientation of Nuclei Following Beta-Decay

In order to establish the necessary asymmetries that can be measured to test for Lorentz Invariance Violation (LIV), an analysis of the way nuclei become oriented following the emission of a β-particle is useful. In this section a theoretical framework of nuclear orientation is presented, without assuming LIV, followed by a general description of the gamma-ray distribution. The specific cases of Cobalt-60 and Sodium-22 as potential source candidates will be discussed. Finally, two side issues will be explored. The first involves an analysis of the Treiman [12] claim, that the extent to which the correlation between γ-emission and recoiling nucleus depends upon the coefficient c may allow for a test of the tensor component of the weak interaction. The second will analyze the case of neutron β-decay, which is a mixed F/G-T transition. It will be assessed to what extent the polarization depends upon the tensor component of the weak interaction.

3.1 Theory of Nuclear Orientation

A description of oriented nuclei can be done with the aid of the parameter $f_k(J)$, which describes the degree of orientation of order k. These parameters characterize the state of orientation of the nuclei, and can be defined as [5]

$$f_k(J) = \binom{2k}{k}^{-1} J^{-k} \sum_m \sum_{\nu=0}^{k} (-1)^\nu \frac{(J-m)!(J+m)!}{(J-m-\nu)!(J+m-k+\nu)!} \binom{k}{\nu}^2 a_m \tag{3.1}$$

Here the term J represents the total angular momentum of the nucleus. The term a_m represents the relative populations of the magnetic sublevels. For a completely polarized nucleus, $a_{m=J} = 1$, and for a completely randomly oriented nucleus $a_m = \frac{1}{2J+1}$, for all m. In the case of alignment, only the absolute value of m is measured and therefore $a_m = a_{-m}$. Assuming that the source parent nuclei in the sample are unoriented, the daughter nucleus will have an alignment along its recoil axis. The distribution of m values along this axis was derived in the previous chapter, and can be written as [6]

$$W(m) = \frac{1}{2J+1}\Big\{1 - (A+B)x_1\frac{m}{J} - \frac{2}{3}cx_2\frac{J(J+1)-3m^2}{J(2J-1)}\Big\} \tag{3.2}$$

Where the coefficients A, B and c are given by Jackson et al [7] and listed in Table 2.1.The polarization can then be calculated as

$$P = \frac{1}{J}\sum_m mW(m) \tag{3.3}$$

If we start with an unoriented nucleus which undergoes β-decay, then the recoiling daughter nucleus will have a polarization along the recoil axis

$$P = -\frac{(A+B)(1+J)}{3J}x_1 \tag{3.4}$$

Where the variable x_1 is defined in Treiman [12]. For a pure Gamow-Teller transition, the sum $A + B$ is zero, and thus there will be no polarization resulting from the nuclear recoil. However it is still possible to define an axis of alignment from the recoil direction. Here alignment is defined as $[3m^2 - J(J+1)]/J(2J-1)$. It ranges between 0 for no alignment, and 1 for complete alignment ($m = \pm J$). For mixed transitions the value $A + B$ may have a finite value, and thus the nucleus may have a polarization.

3.1.1 Change of orientation parameters as a result of γ or β decay

In order to calculate how the $f_k(J)$'s change, it is necessary to calculate how the magnetic substate distributions of the parent and daughter nuclei are related. After a β or γ transition, the probabilities a_{m_i} are connected to a_{m_0} via the relation

$$a_{m_i} = \sum_{m_i} a_{m_0} P_{m_0 m_i} \tag{3.5}$$

Where $\sum_{m_i} P_{m_0 m_i} = 1$. The probabilities P can be written as a function of the transformation coefficients for the addition of angular momentum.

$$P^{(L)} = | < J_i m_i L M | J_i L J j_0 m_0 > |^2 \tag{3.6}$$

A description of the orientation requires a relation between the initial $f_k(J_0)$ and the final $f_k(J_i)$ parameters. This is given as [4]

$$f_k(J_i) = w_k(J_i) w_k(J_0)^{-1} (2J_0 + 1) W(J_i L k J_0; J_i J_0) f_k(J_0) \tag{3.7}$$

Where

$$w_k(J_i) w_k(J_0)^{-1} = \left(\frac{J_0}{J_i}\right)^k \left[\frac{(2J_i + k + 1)!(2J_0 - k)!}{(2J_i - k)!(2J_0 + k + 1)!}\right]^{\frac{1}{2}} \tag{3.8}$$

$$(2J_0 + 1) W(J_i L k J_0; J_i J_0) f_k(J_0) = \left[\frac{(2J_i - L)!(2J_0 - L)!}{(2J_i + L + 1)!(2J_0 + L + 1)!}\right]^{\frac{1}{2}} Y_\nu(J_i k J_0) \tag{3.9}$$

Where the Y_ν's are defined according to [1].

3.2 Angular Distribution of Gamma Radiation of Cobalt-60 and Na-22 in the V-A Regime

3.2.1 Cobalt-60

The decay-scheme for ^{60}Co is shown in figure 3.1. It undergoes a G-T transition from spin-parity 5^+ to 4^+, then emits two E2 gamma rays. For transitions of the type $J_0 \to J_0 - L$, equation 3.7 is dramatically simplified [4] in the following way

$$f_k(J_i) = \frac{J_0^k(2J_0 - k)!}{(2J_0)!} \frac{(2J_i)!}{J_i^k(2J_i - k)!} f_k(J_0) \tag{3.10}$$

or

$$N_k(J_i) f_k(J_i) = N_k(J_0) f_k(J_0) \tag{3.11}$$

Where the N_k's are defined in [5].

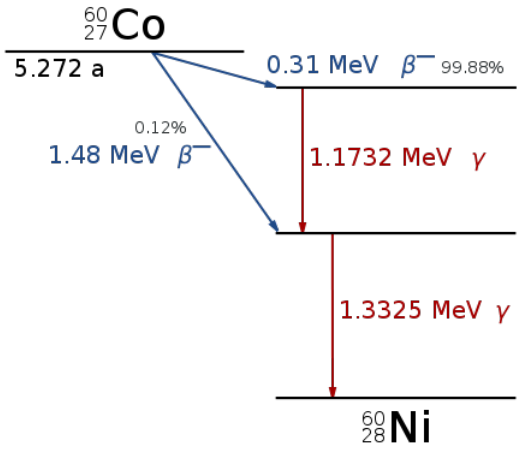

Figure 3.1: The decay scheme for Cobalt-60. Each γ emission is an electric quadrupole (E2) transition

The explicit formula for the angular distribution of the electric quadrupole radiation ($L = 2$) for the transition $J_f = J_i - 2$ is given in [5] as

$$W(\theta) = 1 - \frac{15}{7} N_2 f_2 P_2(\cos\theta) - 5 N_4 f_4 P_4(\cos\theta) \tag{3.12}$$

The coefficients are defined in [5], and the symbolic expressions for f_2,f_4, N_2 and N_4 are reproduced here as

$$f_2 = \left(\frac{1}{J^2}\right)\left[\sum_{m_i} m_i^2 a_{m_i} - \frac{1}{3} J(J+1)\right] \tag{3.13}$$

$$f_4 = \left(\frac{1}{J^4}\right)\left[\sum_{m_i} m_i^4 a_{m_i} - \frac{1}{7}(6J^2+6J-5)\sum_{m_i} m_i^2 a_{m_i} + \frac{3}{35} J(J-1)(J+1)(J+2)\right] \tag{3.14}$$

$$N_2 = \frac{J}{(2J-1)} \tag{3.15}$$

$$N_4 = \frac{J^3}{(J-1)(2J-1)(2J-3)} \tag{3.16}$$

As mentioned above, the transition from 5^+ to 4^+ is a G-T transition, and therefore $A+B=0$. This means the magnetic substate distribution becomes

$$W(m) = \frac{1}{2J+1}\left[1 - \frac{2}{3} c x_2 \left(\frac{J(J+1) - 3m^2}{J(2J-1)}\right)\right] \tag{3.17}$$

The coefficient c can be derived [14], and is equal to $\frac{J(2J-1)}{(J+1)(2J+3)}$. This results in the following amendments to the orientation parameters

$$f_2 = \frac{2(2J-1)}{45J} x_2 \tag{3.18}$$

$$f_4 = 0 \tag{3.19}$$

These are used in Eq. 3.12, and the resulting numerical expression for the angular distribution pattern is

$$W(\theta) = \frac{1}{21}(21 + x_2(1 - 3\cos^2\theta)) \tag{3.20}$$

which is independent of J. x_2 was calculated to be 0.24 for cobalt-60, and the angular distribution plot for the first E2 transition is shown in figure 3.2.

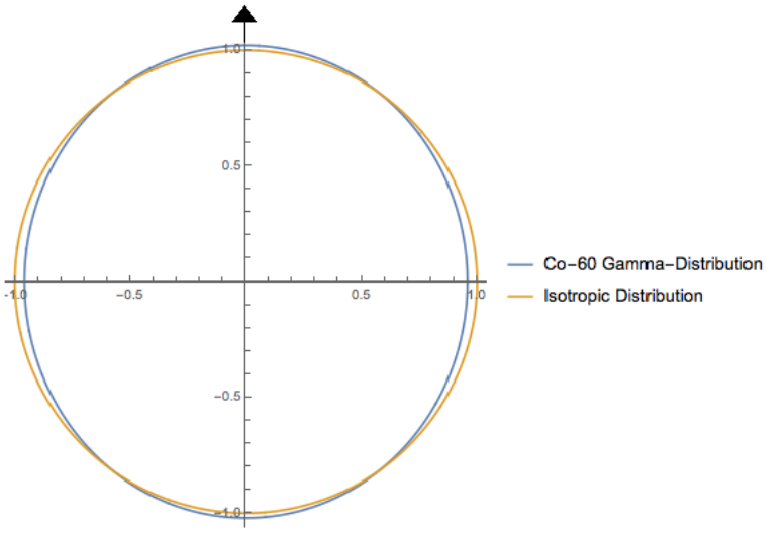

Figure 3.2: The angular distribution pattern for the first E2 transition following β decay of unoriented cobalt-60 nuclei, compared to isotropic case. The arrow represents the recoil direction.

The emission of the first E2 radiation is followed almost immediately by the emission of a second E2 gamma photon. The angular distribution will be identical with the first emission, owing to the independence of J in Eq. 3.20. As can be seen, the gamma-ray distribution is very close to isotropic. The deviation from isotropy was calculated to be 0.017, or less than 2 percent. The difference between the Cobalt-60 γ-distribution and isotropic distribution is plotted in Figure 3.3.

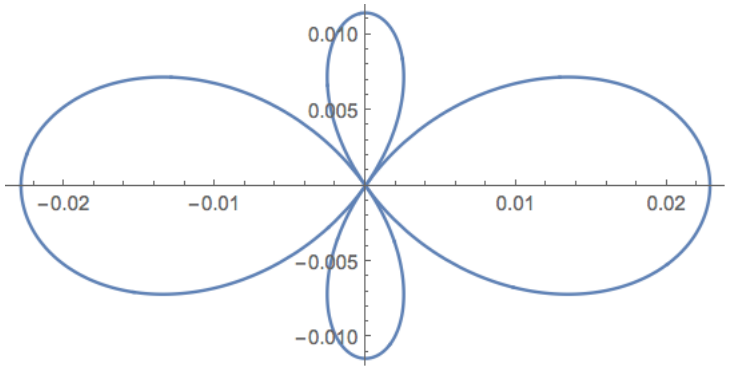

Figure 3.3: Same polar plot as Figure 3.2 (over 2π), with the isotropic part subtracted from the Co-60 γ distribution.

3.2.2 Sodium-22

Sodium undergoes β^+ decay via the transition $3^+ \rightarrow 2^+$, followed by a single electric quadrupole transition (E2) from $2^+ \rightarrow 0^+$. The decay scheme is shown in figure 3.4.The angular distribution pattern can be found using Eq. 3.20, with a value of $x_2 = 0.31$. The result is plotted below in figure 3.5. The anisotropic distribution here is again very weak. Deviation from isotropy was calculated to be 0.022, or slightly more than 2 percent.

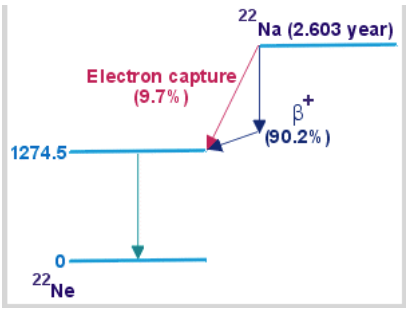

Figure 3.4: Decay scheme for ^{22}Na, which undergoes β^+ decay followed by an electric quadrupole transition Source:`http://ns.ph.liv.ac.uk/~ajb/radiometrics/glossary/images/na_decay.gif`

The difference between the Sodium-22 γ-distribution and isotropic distribution is plotted in Figure 3.6.

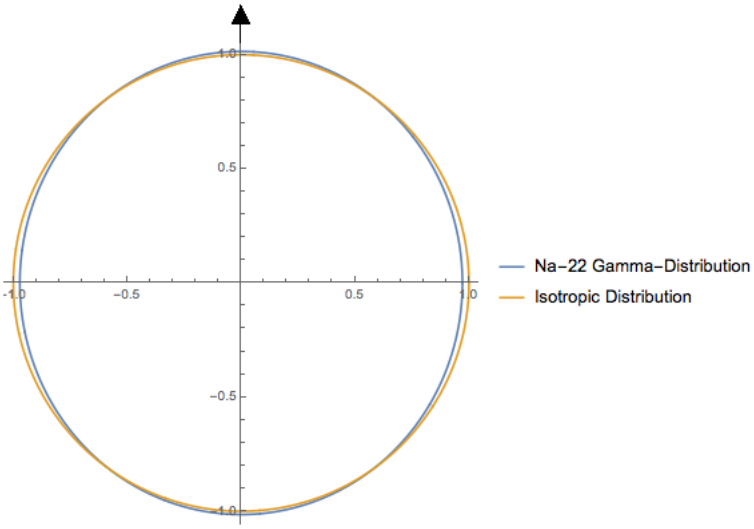

Figure 3.5: The angular distribution pattern for the E2 transition following β^+ decay of sodium-22. The arrow represents the recoil direction.

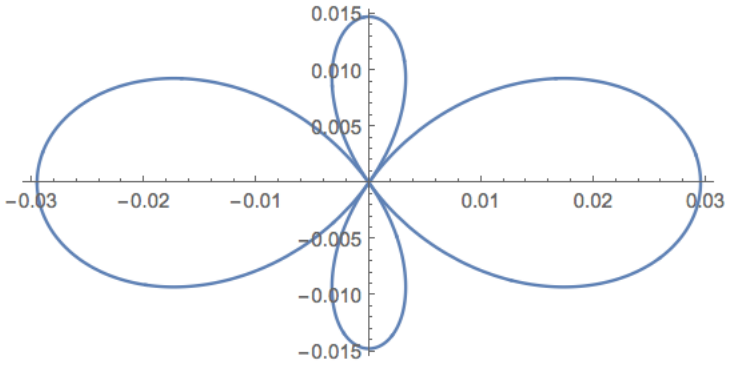

Figure 3.6: Same polar plot as Figure 3.5 (over 2π), with the isotropic part subtracted from the Na-22 γ distribution.

3.3 Effect on Nuclear Orientation and Gamma-Distribution by Assuming a Tensor Component in Weak Interaction

The motivation behind the analysis of this chapter has been that the recoiling nucleus will have an alignment (or polarization) along the axis of flight. If the nucleus then undergoes gamma-decay, there will be a correlation between this emission and the recoil direction. It has been suggested by Treiman [12] that the extent to which this effect depends upon the coefficient c may allow for a test of the tensor contribution to the weak interaction. Here a brief analysis of this claim is made.

The coefficients A, B and c were solved assuming only a tensor contribution. This involved dealing with α_L and α_R in the alphabet soup [14]. The coefficients then turn out to be

$$A = \pm\lambda_{j'j}\frac{|\alpha_L|^2 - |\alpha_R|^2}{|\alpha_L|^2 + |\alpha_R|^2} \tag{3.21}$$

$$B = \pm\lambda_{j'j}\frac{|\alpha_L|^2 - |\alpha_R|^2}{|\alpha_L|^2 + |\alpha_R|^2} \tag{3.22}$$

$$c = \Lambda_{j'j} \tag{3.23}$$

Here the plus sign refers to electron emission, and the minus sign refers to positron emission. If we assume α_R is zero, then the expressions for A and B reduce to $\pm\lambda_{J'J}$. For transitions of the form $J \to J' = J + 1$, $\pm\lambda_{J'J} = \mp J/J{+}1$, and for the coefficient c, $\Lambda_{J'J} = J(2J{-}1)/(J{+}1)(2J{+}3)$. Therefore $A{+}B = \pm 2\lambda_{J'J} = \pm 2J/J{+}1$, which is non-zero, unlike the $\mathbf{V}-\mathbf{A}$ case. This has consequences for the polarization (Eq. 3.4), which can now be written as

$$P = \pm\frac{2}{3}x_1 \tag{3.24}$$

However for the polar plot (Eq. 3.12), f_4 is still zero because the term with $(A + B)$ involves a sum over odd m, which will be zero if we start with an unoriented nucleus. The coefficient c differs from the $\mathbf{V}-\mathbf{A}$ case by a sign change, however because f_2 remains the same in both $\mathbf{T}$ and $\mathbf{V} - \mathbf{A}$ (and

importantly independent of c), the distributions for cobalt-60 and sodium-22, and hence the deviation from isotropy, will be the same. Hence the sign change in c, as a result of going from $\mathbf{V} - \mathbf{A}$ to $\mathbf{T}$, cannot be measured by looking at the gamma ray distribution.

3.4 Effect on Neutron Polarization of assuming Tensor Component in Weak Interaction

Neutron β-decay is a mixed Fermi/Gamow-Teller transition. $M_{GT} = \sqrt{3}$ and $M_F = 1$. We again look at the coefficients in the alphabet soup [14], and solve them assuming only a tensor component. Taking $\alpha_R = 0$, the coefficients A, B and c become

$$A = +\frac{2}{3} \tag{3.25}$$

$$B = +\frac{2}{3} \tag{3.26}$$

$$c = 0 \tag{3.27}$$

The c coefficient disappears for $J = \frac{1}{2}$, as can be seen by looking at the alignment term in Eq. 3.2. The denominator goes to ∞ and therefore the coefficient must go to zero. This means that there is no alignment of the neutron following β-decay. Looking at the polarization (Eq. 3.4), we see that it becomes

$$P = -\frac{4}{3}x_1 \tag{3.28}$$

were x_1 is given in [12]. Therefore we see significant polarization as a result of assuming only the tensor component.

Chapter 4

Measuring Lorentz Invariance Violation

In order to perform an experiment to measure LIV, several issues need to be addressed. In this chapter, the angular distribution of γ-radiation from polarized nuclei is derived using the LIV formalism. This is required in order to define the observables which will be used in the proposed experiment. A schematic set-up of the detectors is described, as well as a discussion of the coordinate system in which $\vec{\chi}$ will be measured. Finally, the variation in the asymmetry as a function of sidereal time is calculated and plotted.

4.1 Decay Rate Distribution in LIV Regime

Treiman's original idea was to see if the weak interaction contained Vector ($\mathbf{V}$) and/or Axial-Vector ($\mathbf{A}$), which could be determined from the sum $A + B$. Another possibility, and one relevant to the current study, would be to measured the γ-ray distribution relative to the recoiling nucleus. The current study of Lorentz Invariance Violation (LIV) would benefit from Treiman's proposal. In this case the polarization axis would be defined along some preferred direction in space. We start with the expression for the Gamow-Teller transition rate of polarized nuclei (Eq. 37 in [11]), which is reproduced below

$$d\Gamma_{GT} = d\Gamma_0 \left\{ \left[1 - \frac{2}{3}\chi_r^{00} + \frac{2}{3}(\chi_r^{l0} + \tilde{\chi}_i^l)\frac{p^l}{E_e} \right] \right.$$
$$\mp \Lambda^{(1)} \left[(1 - \chi_r^{00})\frac{p \cdot \hat{I}}{E_e} + \tilde{\chi}_i^l \hat{I}^l + \chi_r^{lk}\frac{p^l \hat{I}^k}{E_e} - \chi_i^{l0}\frac{(p \times \hat{I})^l}{E_e} \right] \tag{4.1}$$
$$\left. + \Lambda^{(2)} \left[-\chi_r^{00} + (\chi_r^{l0} + \hat{\chi}_i^l)\frac{p^l}{E_e} + 3\chi_r^{kl}\hat{I}^k\hat{I}^l - 3\chi_r^{l0}\hat{I}^l\frac{p \cdot \hat{I}}{E_e} - 3\chi_i^{ml}\hat{I}^m\frac{(p \times \hat{I})^l}{E_e} \right] \right\} .$$

In the proposed experiment, we are not measuring the electron (positron) momentum, and therefore it is necessary to integrate over this variable (p_e). Terms with p are odd functions, and thus will drop out following integration. In addition, we neglect the term χ_r^{00}, as this is only measured by comparing 2 decays moving at different velocities. We are then left with the LIV decay rate expression

$$\Gamma_{LIV} = X\left[1 \mp \Lambda^{(1)}[\tilde{\chi}_i^l] + \Lambda^{(2)}[3\chi_r^{kl}\hat{I}^k\hat{I}^l]\right] \tag{4.2}$$

where X is the integral over phase space. This factor can be removed by taking the ratio of the LIV decay rate expression, with that predicted from the Standard Model

$$\frac{\Gamma_{\rm LIV}}{\Gamma_{\rm SM}} = 1 \mp \Lambda^{(1)}\tilde{\chi}_i^l\hat{I}^l + \Lambda^{(2)}\chi_r^{lk}\hat{I}^l\hat{I}^k. \tag{4.3}$$

The terms $\Lambda^{(1)}$ and $\Lambda^{(2)}$ are related to polarization and alignment respectively. Thus we can relate Eq. 4.3 with the coefficients of the alphabet soup, which gives

$$\frac{\Gamma_{\rm LIV}}{\Gamma_{\rm SM}} = 1 \mp A\frac{\langle m \rangle}{J}\tilde{\chi}_i^l\hat{I}^l + c\frac{J(J+1) - \langle m^2 \rangle}{J(2J-1)}\chi_r^{ll}\hat{I}^l. \tag{4.4}$$

To simplify things, we look at only the diagonal components of the tensor. Later we will make a simplification and treat the diagonal components (ignoring the χ_r^{00} term) as a 3-vector, with real spacial components. It should be noted here that this step is non-trivial, and the details are not treated in this thesis. If we then start with an unpolarized sample of nuclei, the polarization will be along $\tilde{\chi}_i^l$, and the alignment will be along χ_r^{ll}. Each component will be measured separately. For polarization, the m state distribution takes the form

$$W(m) = \frac{1}{2J+1}\left(1 + A\frac{m}{J}|\vec{\tilde{\chi}}_i|\right) \tag{4.5}$$

and for alignment it becomes

$$W(m) = \frac{1}{2J+1}\left(1 + c\frac{J(J+1) - 3m^2}{J(2J-1)}|\vec{\chi}_r|\right) \tag{4.6}$$

By analogy with Eq. 14 in [12], we write the polarization as a result of LIV as

$$P = -\frac{(J+1)}{3J}A|\vec{\tilde{\chi}}_i| \tag{4.7}$$

Notice here that in the LIV case, as opposed to the case discussed in chapter 3, the polarization does not vanish. However by only measuring the γ-photons, we are still unable to measure this polarization, only the alignment. The γ-ray distribution was discussed in Chapter 3, and the formula for the E2 transition $J_f \to J_i = J_f - 2$ is given as

$$W(\theta) = 1 - \frac{15}{7}N_2 f_2 P_2 - 5N_4 f_4 P_4 \tag{4.8}$$

where the N_i's are the normalization factors, and P_n are the Legendre polynomials. The orientation parameters f_i now become

$$f_2 = \frac{2J-1}{15J}|\vec{\chi}_r| \tag{4.9}$$

$$f_4 = 0 \tag{4.10}$$

With this the angular distribution in the γ's assuming a LIV-violating term becomes

$$W(\theta) = \frac{1}{14}\left[14 + |\vec{\chi}_r|(1 - 3\cos^2\theta)\right] \tag{4.11}$$

This leads to a maximal asymmetry

$$A_\gamma = \frac{W(0) - W(\frac{\pi}{2})}{W(0) + W(\frac{\pi}{2})} \approx -\frac{3}{28}|\vec{\chi}_r| \tag{4.12}$$

Which corresponds to a maximum sensitivity of about 10 percent. The derivations above allow us to infer to some extent what happens if one does

not measure the recoil direction, but there is Lorentz Violation. The equivalent idea in going from Eq. (2.7) to Eq. (2.9) will play a role.

4.2 Statistical Analysis

The current upper bounds on $X_r^{\mu\nu}$ can be found in [11]. For the current study we are only interested in the diagonal elements. The constraints for X_r^{ll} (χ_r^{ll} boosted to Sun-centered frame), currently stands at 10^{-6}. In the proposed experiment, we wish to improve this upper bound by at least an order of magnitude. To measure the degree of alignment, we defined the maximal asymmetry as

$$A_\gamma = \frac{W(0) - W(\frac{\pi}{2})}{W(0) + W(\frac{\pi}{2})} \tag{4.13}$$

This can be translated to an asymmetry concerning the measured photon count rate N of the detectors as

$$A_\gamma = \frac{N_1 - N_2}{N_1 + N_2} \tag{4.14}$$

which will vary depending on the direction of $|\vec{\chi}|$, and the orientation of the detectors. The analysis of gamma-decay involves counting (poisson) statistics. A poisson process involves randomly distributed occurrences in some variable, with the number of occurrences being statistically independent. In general we write the number of expected events between times t_1 and t_2 as

$$\mu = \int_{t_1}^{t_2} \Gamma(t) dt \tag{4.15}$$

Due to the randomness of the events, the count rate N must be in the region of μ, with the probability distribution given as

$$P(N) = e^{-\mu} \frac{\mu^N}{N!} \tag{4.16}$$

For sufficiently large μ the probability distribution function can be written as a Gaussian

$$P_g(N) = \frac{1}{\sqrt{2\pi\mu}} \exp\left(- \frac{(N-\mu)^2}{2\mu} \right) \tag{4.17}$$

Normally the true mean is unknown. Therefore using the principle of maximum likelihood the measured value N is taken as a best estimate of this quantity. The standard deviation $\sigma = \sqrt{N}$.

We want the fractional uncertainty in N to be smaller than the desired upper bound we want to achieve for χ_r^{ll}. In other words $1/\sqrt{N} < 10^{-7}$. This means we need a count rate $N > 10^{14}$. However various factors, such as detector sensitivity, will increase the required number of counts.

In calculating the asymmetry A_γ, there will be an associated error which depends upon the individual error in count rate from each detector. Let N_1 be the detector (or series of detectors) positioned at the 'equatorial', and let N_2 be the detector (or series of detectors) positioned at each 'pole'. The formula for error propagation can be calculated from

$$\delta A_\gamma = \sqrt{\left(\frac{\partial A_\gamma}{\partial N_1}\delta N_1\right)^2 + \left(\frac{\partial A_\gamma}{\partial N_2}\delta N_2\right)^2} \tag{4.18}$$

Which leads to a relative error in the asymmetry of

$$\delta A_\gamma = 2 \cdot \sqrt{\frac{N_1 N_2}{(N_1+N_2)^3}} \tag{4.19}$$

Which reduces to $1/\sqrt{2N}$ assuming N_1 and N_2 are approximately the same.

4.3 Detector Set-Up

4.3.1 Optimizing Detector Opening Angle

The counts N_1 and N_2 can be related to the detector efficiency ϵ as $ST \cdot \epsilon_1^\gamma$ and $ST \cdot \epsilon_2^\gamma$ respectively. S represents the activity of the source in Becquerels, and T is the measurement time. ϵ_1^γ and ϵ_2^γ are proportional to integrating Eq. 4.15 over a solid angle Ω. Thus the asymmetry becomes

$$A_\gamma = \frac{\int_a^b W(\theta)d\Omega - \int_c^d W(\theta)d\Omega}{\int_a^b W(\theta)d\Omega + \int_c^d W(\theta)d\Omega} \tag{4.20}$$

Here we assume that the detectors will be the circular base of a cone, in which case we require an integration over spherical coordinates. The integral $\int_a^b W(\theta)d\Omega$ can be straightforwardly evaluated, with $d\Omega = sin(\theta)d\theta d\phi$. The second integral $\int_c^d W(\theta)d\Omega$ requires a substitution of angles. We define $\vec{y}$ as the vector with angle α relative to the y-axis and the angle β in the x-z plane (equivalent to θ and ϕ in the usual spherical coordinates). $\vec{y}$ makes an angle with the z-axis of $\cos^{-1}[\sin(\alpha)cos(\beta)]$. Replacing θ as defined in Eq. 4.15 with this angle, and integrating over the solid angle defined as $d\Omega = \sin(\alpha)d\alpha d\beta$, we get the desired result. Thus our two efficiencies become

$$\epsilon_1^\gamma = \frac{1}{28}\pi\big[56 - (56 + |\vec{\chi}_r|)\cos(\theta_0) + |\vec{\chi}_r|\cos(3\theta_0)\big] \tag{4.21}$$

$$\epsilon_2^\gamma = \frac{1}{14}\pi\big[56 + |\vec{\chi}_r|(1 + 2\cos(\theta_0) + \cos(2\theta_0))\big]\sin^2\left(\frac{\theta_0}{2}\right) \tag{4.22}$$

where θ_0 is defined as the opening angle of the detectors. The asymmetry can be calculated by taking the difference over the sum as was done in Chapter 3. After simplifying the expression becomes

$$A_\gamma = -\frac{3}{28}|\vec{\chi}_r|\cos^2\left(\frac{\theta_0}{2}\right)\cos(\theta_0) \tag{4.23}$$

The asymmetry can be plotted as a function of the opening angle θ_0, and is shown in figure 4.1. As can be seen, at $\theta_0 = 0$, the maximal asymmetry of about 10 percent is achieved. This drops to zero for $\theta_0 = \pi/2$.

It should be noted that in practice θ_0 can only be as large as $\pi/4$, with an opening angle of $\pi/2$. Taking $\theta_0 = \pi/4$ yields the best statistics, as it optimizes the trade off between count rate and asymmetry sensitivity.

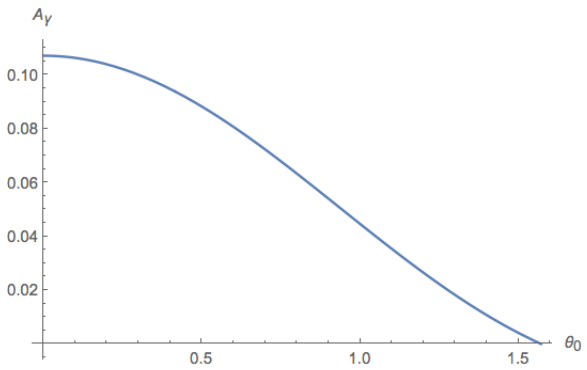

Figure 4.1: The asymmetry in the gamma distribution, measured as a function of opening angle

4.3.2 Detector Orientation

It has been concluded [13], based on geometrical arguments, that the optimal detector set-up is that shown in Figure 4.2. The detectors use ZnSe(Te) as scintillation crystals, and converts low energy photons into a current using Silicon photodiodes. This current will then be proportional to the count rate.

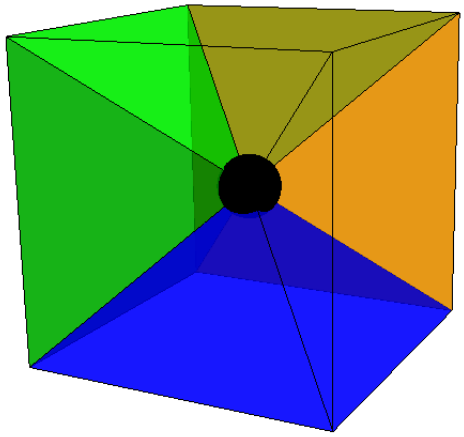

Figure 4.2: The pyramidal detector setup. Each detector covers a solid-angle of $\frac{2\pi}{3}$.

The roles of the detectors can be gauged from Figure 4.3. For clarity the third axis, pointing parallel to the Earth's spin axis, has not been included. This is because the count rate for this detector should not vary with sidereal

time.

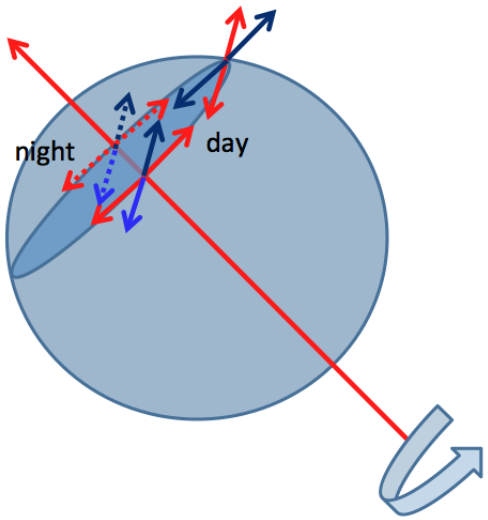

Figure 4.3: The simplified detector setup. Two detectors are positioned along an axis perpendicular to the Earth's rotation axis. The other two are placed along the 'East-West' direction. It can be seen that after 6 hours the roles of the detectors will be interchanged, which will lead to a unique sidereal dependence for the asymmetry.

4.4 The Sun-Centered Inertial Reference Frame

In comparing limits on the Lorentz invariance-violating tensor, it is helpful to define a single inertial reference frame in which to report all findings. This frame is known as the Sun-centered frame. Generally speaking, the preferred direction will point in different directions depending on which reference frame one uses. It is therefore more likely that the LIV tensor has constant values in a frame which has approximately fixed orientation and velocity in space. The orbit of the Earth in this frame is given in [2], and is reproduced in Figure 4.4.

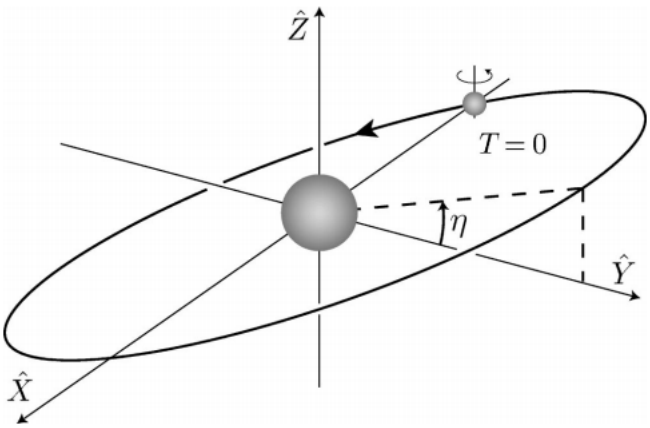

Figure 4.4: Orbit of Earth in Sun-centered frame.

The origin of this frame is the center of the Sun, with the $\hat{Z}$-axis pointing along the Earth's rotation axis. The $\hat{X}$-axis points along the vernal equinox on the celestial sphere, and the $\hat{Y}$-axis completes the right handed coordinate system. Strictly speaking, the orientation of the Sun-centered frame is not fixed, due to the fact that the Earth's precesses about it's rotation axis, but for the purposes of most experiments the effect is negligible.

If we ignore the velocity of the Earth, and assume translational invariance, we can move the Sun-centered frame to the center of the Earth. This allows for a more direct method is seeing the relationship between this frame and that of the laboratory, and is shown in Figure 4.5.

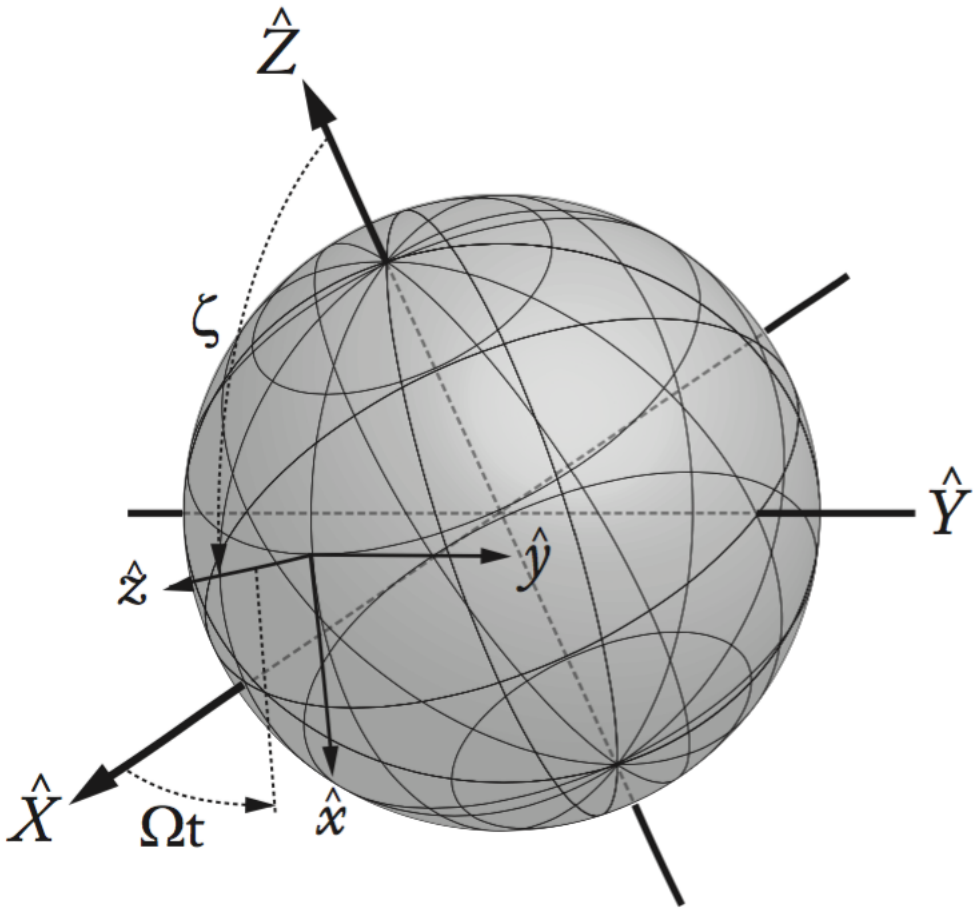

Figure 4.5: The laboratory frame, with coordinates ($\hat{x}$,$\hat{y}$,$\hat{z}$), and the Sun-centered frame, with coordinates ($\hat{X}$,$\hat{Y}$,$\hat{Z}$).

4.5 Sidereal Dependence

In order to derive the sidereal dependence of the asymmetries between the detectors, we first define $\vec{\chi}$ in the Sun-centered frame. Using spherical coordinates, the preferred direction assumes the form

$$\vec{\chi}_{sun} = \begin{bmatrix} \sin\theta_n \cos\phi_n \\ \sin\theta_n \sin\phi_n \\ \cos\theta_n \end{bmatrix} \tag{4.24}$$

A rotation matrix is used to express the laboratory coordinates in terms of the Sun-centered ones. This transformation can be achieved with the following matrix

$$R(\zeta, t) = \begin{bmatrix} \cos\zeta\cos\Omega t & \cos\zeta\sin\Omega t & -\sin\zeta \\ -\sin\Omega t & \cos\Omega t & 0 \\ \sin\zeta\cos\Omega t & \sin\zeta\sin\Omega t & \cos\zeta \end{bmatrix} \tag{4.25}$$

where ζ is the co-latitude of the experiment and $\Omega = 2\pi/(23h56m)$. Thus the preferred direction in the laboratory frame can be written as

$$\vec{\chi}_{lab} = \begin{bmatrix} -\cos\theta_n \sin\zeta + \cos\Omega t\cos\phi_n \sin\theta_n + \cos\zeta\sin\Omega t\sin\theta_n\sin\phi_n \\ -\cos\phi_n\sin\Omega t\sin\theta_n + \cos\Omega t\sin\theta_n\sin\phi_n \\ \cos\zeta\cos\theta_n + \cos\Omega t\cos\phi_n\sin\zeta\sin\theta_n + \sin\Omega t\sin\zeta\sin\theta_n\sin\phi_n \end{bmatrix} \tag{4.26}$$

If we assume the orientation of the detectors described in Figure 4.3, then $\zeta = \pi/2$ and $\vec{\chi}_{lab}$ assumes the simplified form

$$\vec{\chi}_{lab} = \begin{bmatrix} -\cos\theta_n + \cos\Omega t\cos\phi_n \\ -\cos\phi_n\sin\Omega t\sin\theta_n + \cos\Omega t\sin\theta_n\sin\phi_n \\ \cos\Omega t\cos\phi_n\sin\theta_n + \sin\Omega t\sin\theta_n\sin\phi_n \end{bmatrix} \tag{4.27}$$

The two variables that determine the direction of $\vec{\chi}$ are θ_n and ϕ_n (the angles with respect to the Sun-centered coordinate system), with Ω being a constant value, and ζ being set by the co-latitude of the experiment. Therefore the asymmetries between the detectors will vary depending on the direction of $\vec{\chi}$. For illustrative purposes the asymmetries for 3 preferred directions (along each axis in the Sun-centered frame) are shown in Figures 4.6, 4.7 and 4.8.

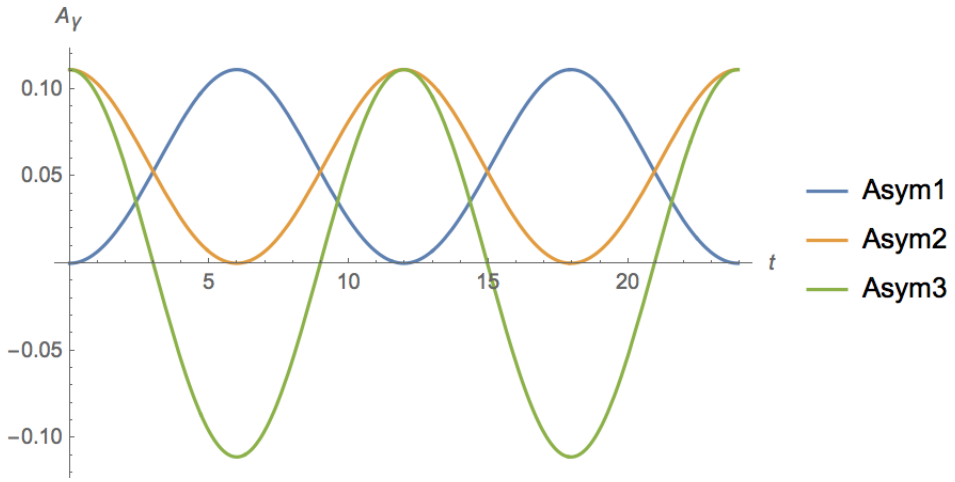

Figure 4.6: The 3 asymmetries between the principle detector axes as a function of sidereal time, assuming $\vec{\chi}$ points along the $\hat{X}$-direction in the Sun-centered frame. Asym1,Asym2 and Asym3 refer to the asymmetries between the $\hat{x} - \hat{y}$,$\hat{x} - \hat{z}$, and $\hat{y} - \hat{z}$ detectors respectively, given along the axes defined in the laboratory frame. Here $\hat{z}$ points towards the azimuth (perpendicular to the Earth's rotation axis), $\hat{x}$ points directly South, and $\hat{y}$ completes the right handed coordinate system. Here we take $|\vec{\chi}| = 1$.

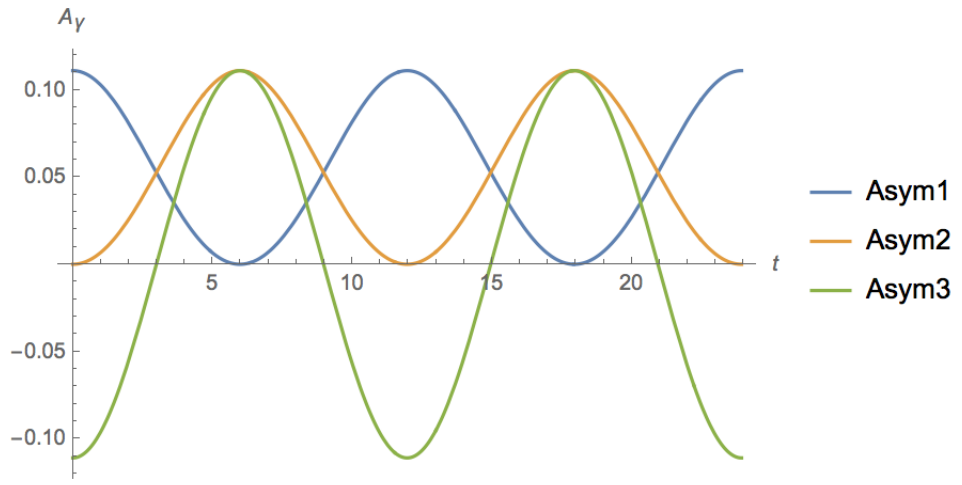

Figure 4.7: The 3 asymmetries between the principle detector axes as a function of sidereal time, assuming $\vec{\chi}$ points along the $\hat{Y}$-direction in Sun-centered frame. Asym1,Asym2 and Asym3 are defined as above.

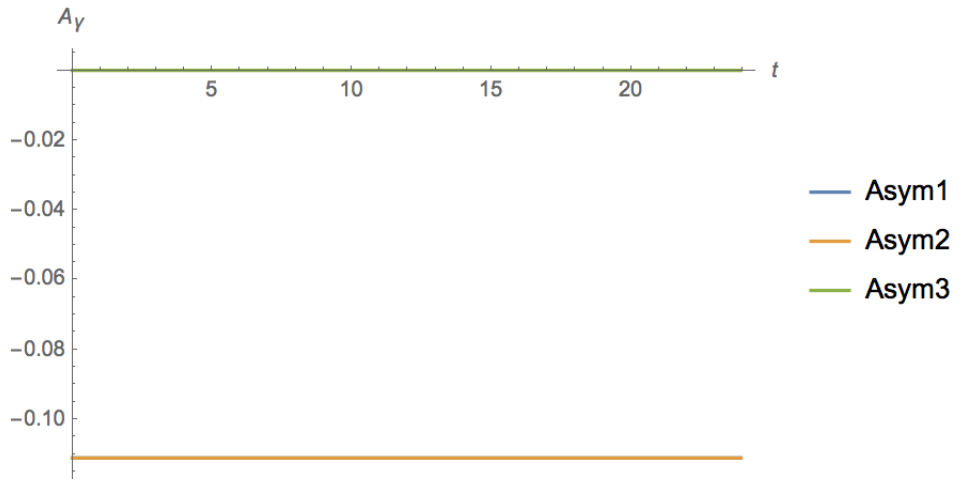

Figure 4.8: The 3 asymmetries between the principle detector axes as a function of sidereal time, assuming $\vec{\chi}$ points along the $\hat{Z}$-direction in Sun-centered frame. Asym1,Asym2 and Asym3 are defined as above.

As can be seen in Figure 4.8, in the unfortunate case that $\vec{\chi}$ points along

the $\hat{Z}$-direction, there will be no variation with the Earth's rotation. Therefore measuring LIV in this scenario will require a different detector set-up, such as one that rotates independently of the Earth's sidereal frequency. From Figures 4.6 and 4.7 the unique LIV signal can be seen, in the form of a doubling of the asymmetry oscillation within the sidereal day.

Chapter 5

Conclusion and Outlook

In this thesis we studied the possibility of measuring Lorentz Invariance Violation (LIV) by observing the distribution of γ-rays from nuclei that have undergone β-decay. The motivation for this inquiry was Treiman's [12] suggestion that nuclei can become polarized (or aligned) along the recoil axis following the emission of a β-particle. We applied this claim to the case were we do not measure the recoil direction, but there is a preferred direction in space. We identified Co-60 and Na-22 as suitable isotopes to test for LIV.

The goal of the experiment proposed in this study is to increase the current best upper bounds on the real diagonal elements of the Lorentz-violating tensor $\chi^{\mu\nu}$, which currently stands at 10^{-6}, by an order of magnitude. It was mentioned in Chapter 4 that the required number of counts to achieve the necessary statistical precision would need to be larger than 10^{14}. Various factors which were not discussed here, such as the detector sensitivity, would lead to a higher required count rate. It has been calculated [13], assuming one requires 10^{16} counts, that 9.3 μg of Na-22 and 24 μg of Co-60 are required to achieve the required statistical accuracy. The activities, in Curie, are 58 mCi and 27 mCi respectively. The measuring time is approximately 1 year. Additionally, it should be noted that Co-60 undergoes 2 consecutive γ-decays following β-decay. This will then yield twice the number of γ's, and therefore will double the statistical accuracy.

Another issue which was not addressed in detail was the intermediate state in the decay of both isotopes. If the time evolution of this state significantly alters the initial polarization of the nucleus following β-decay, this will affect the LIV measurement. The main source of such a possible alteration comes from the Earth's magnetic field, in which the nuclear spin precesses.

We can calculate how this precession will affect the polarization direction by looking at the condition

$$\tau\omega_L = \frac{2\tau\mu B}{\hbar} \gg 1 \tag{5.1}$$

Here τ is the intermediate state lifetime, ω_L is the Larmor precession frequency, μ is the magnetic moment of the nucleus, and B is the magnetic field of the Earth. The values for the intermediate states of both isotopes were calculated in [13] and they were found to lead to no appreciable change in the nuclear spin compared to the lifetime of the intermediate state.

Finally, we turn to the issue of the detector orientation and setup. This was discussed in detail in Chapter 4. The setup we chose was one in which the laboratory frame was fixed to the Earth's surface, and which revolved with the sidereal frequency. However there are other possible configurations which are complimentary to our suggested setup. If $\vec{\chi}$ points along the Earth's spin direction, then these other configurations must be considered. One such configuration involves a detector setup based in space. The ISS permits the possibility of testing for LIV in low-Earth orbit [8]. The ISS operates in different flight modes, which then allows for different laboratory configurations in the Sun-centered frame. This could then lead to different sensitivities for different components of the Lorentz-violating tensor.

Having considered the various issues in measuring LIV, it can be concluded that the proposed experiment is not simply academic, and can be performed in most standard laboratory settings. There are some logistical issues regarding the measurement time of 1 year. Any bi-daily systemic error, such as a temperature change between night and day that may impact the proper functioning of the detectors, would be compensated for with the unique LIV-signal (doubling of the period of oscillation within the sidereal day) that would be measured in this case. We conclude this thesis with a recommendation for further research into the technical aspects of such an experiment, including a more detailed feasibility study.

Bibliography

[1] LC Biedenharn, J Mi Blatt, and ME Rose. Some properties of the racah and associated coefficients. *Reviews of Modern Physics*, 24(4):249, 1952.

[2] Robert Bluhm, V Alan Kostelecký, Charles D Lane, and Neil Russell. Probing lorentz and cpt violation with space-based experiments. *Physical Review D*, 68(12):125008, 2003.

[3] Don Colladay and V Alan Kostelecký. Cpt violation and the standard model. *Physical Review D*, 55(11):6760, 1997.

[4] JAM Cox and HA Tolhoek. Gamma radiation emitted by oriented nuclei the influence of preceding radiations; the evaluation of experimental data. *Physica*, 19(1):673–682, 1953.

[5] SR De Groot, HA Tolhoek, and WJ Huiskamp. Orientation of nuclei at low temperatures. In *Alpha-, beta-and gamma-ray spectroscopy*, volume 1, page 1199, 1965.

[6] H Frauenfelder, JD Jackson, and HW Wyld Jr. Polarization effects following beta decay. *Physical Review*, 110(2):451, 1958.

[7] JD Jackson, SB Treiman, and HW Wyld. Coulomb corrections in allowed beta transitions. *Nuclear Physics*, 4:206–212, 1957.

[8] V Alan Kostelecký and Matthew Mewes. Signals for lorentz violation in electrodynamics. *Physical Review D*, 66(5):056005, 2002.

[9] V Alan Kostelecký and Stuart Samuel. Spontaneous breaking of lorentz symmetry in string theory. *Physical Review D*, 39(2):683, 1989.

[10] Brian R Martin. *Nuclear and particle physics: An introduction*. John Wiley & Sons, 2006.

[11] JP Noordmans, HW Wilschut, and RGE Timmermans. Lorentz violation in neutron decay and allowed nuclear β decay. *Physical Review C*, 87(5):055502, 2013.

[12] SB Treiman. Recoil effects in k capture and β decay. *Physical Review*, 110(2):448, 1958.

[13] M Vogelzang. Liv in weak interaction. 2016.

[14] KK Vos, HW Wilschut, and RGE Timmermans. Symmetry violations in nuclear and neutron β decay. *Reviews of Modern Physics*, 87(4):1483, 2015.